Estimating the Transmittance of Visible Solar Radiation in the Upper Ocean Using Secchi Disk Observations

Zhongping Lee[1] [iD] , **Shaoling Shang[2]** [iD] , **Keping Du[3], Gong Lin[2], Tongtong Liu[2], and Laura Zoffoli[1,4]** [iD]

[1]School for the Environment, University of Massachusetts Boston, Boston, MA, USA, [2]State Key Lab of Marine Environmental Science, Xiamen University, Xiamen, China, [3]Key Laboratory for Remote Sensing of Environment and Digital Cities, Faculty of Geographical Science, Beijing Normal University, Beijing, China, [4]Mer Molécules, Facultés des Sciences et Techniques, Université de Nantes, Nantes, France

Abstract Penetration of visible solar radiation (VSR) drives heating and phytoplankton photosynthesis in the upper water column; thus, it is always important to accurately describe the vertical distribution of VSR in the oceans. Before the invention and application of modern optical-electronic instruments to measure the vertical profiles of VSR, the transmittance of VSR from surface to deeper ocean (T_{VSR}) was commonly estimated based on water types and subsequently incorporated in dynamic ocean circulation models. However, the measurement of Secchi disk depth (Z_{SD}) has been carried out since the 1860s and there are about a million of Z_{SD} data available for the global oceans. Because Z_{SD} represents a measure of water's transparency, here we present a scheme based on radiative transfer to accurately estimate T_{VSR} with Z_{SD} as the sole input. It is found that the median ratios between modeled and measured T_{VSR} are ~0.8–1.0 for T_{VSR} in a range of 1–100% for measurements made in coastal waters and oceanic gyres. However, this median ratio spans ~0.04–1.0 for the same measurements when the classical water-type-based model was applied. These results suggest a great advantage, and potentially significant impact, in incorporating the volumetric Z_{SD} data to model the dynamic ocean–atmosphere systems in the past 100+ years.

Plain Language Summary Based on radiative transfer and using numerically simulated data, the transmittance (T_{VSR}) of visible solar radiation (VSR) is modeled as a function of Secchi disk depth (Z_{SD}). This scheme was further evaluated using data from numerical simulations and from field measurements where Z_{SD} spans a range of ~1–75 m. For waters from coastal to super blue oceanic gyres, the modeled T_{VSR} agree with measured T_{VSR} very well for T_{VSR} greater than 1%. For the same data set, however, the modeled T_{VSR} can be 20 times lower than measured T_{VSR} for oceanic waters when it was estimated based on the traditional water-type approach. Better modeled T_{VSR} can improve general ocean circulation models, which opens a door to better study the ocean–atmosphere systems in the past decades to a century with the large volume of Z_{SD} data.

1. Introduction

Solar radiation is the key driving force of the Earth system. In particular, the portion in the visible domain (~400–700 nm) that can penetrate into deeper ocean is critical to fuel the "biological pump" via phytoplankton photosynthesis (Falkowski and Wilson, 1992) and to heat the upper ocean through the absorption of photon energy by constituents in water (Lewis et al., 1990; Sathyendranath et al., 1991). All these processes have profound impact to the ocean and atmosphere systems; therefore, a component to represent the vertical profile of visible solar radiation (VSR) has been included in ocean general circulation models since the 1980s (Mellor, 2002; Oberhuber, 1992), especially the widely used ROMS (Hedström, 2000).

Fundamentally, the propagation of solar radiation in water is spectrally selective, where blue photons can penetrate much deeper than red photons in oceanic waters. Therefore, for precise description of the distribution of solar radiation in the upper water column, a full-scale, hyperspectral, numerical model of the radiative transfer in ocean (e.g., Hydrolight) should be used (Mobley et al., 2015; Mobley & Boss, 2012; Mobley & Sundman, 2013). But such a scheme requires extremely high computational power that is not practical for large-scale, high-resolution, ocean circulation modeling. As a compromise, the full-spectral solar radiation is commonly divided into two portions in ocean circulation models, with one for the

visible solar radiation (VSR; ~400–700 nm) and the other for the solar radiation of wavelengths longer than 700 nm (the IR-SWIR domain; Morel & Antoine, 1994). The radiation in IR-SWIR domain is quickly absorbed in the upper ~2 m due to the strong absorption by water molecules (Morel & Antoine, 1994; Simonot & Treut, 1986), so the handling of this portion is relatively simple. For radiation in the visible domain, however, because its transmittance is strongly dependent on constituents in water, different schemes have been developed and implemented in ocean circulation models in the past decades (Gnanadesikan & Anderson, 2009; Kara et al., 2005; Murtugudde et al., 2002).

Generally, the vertical distribution of VSR ($E_{VSR}(z)$) in the upper water column is determined by its surface value ($E_{VSR}(0)$) and the transmittance of VSR (T_{VSR}),

$$E_{VSR}(z) = E_{VSR}(0) \times T_{VSR}(z). \tag{1}$$

Decades of studies have shown that $E_{VSR}(0)$ can be well modeled based on Sun position, atmospheric properties, and cloud information (Frouin et al., 1989). T_{VSR} generally follows an exponential decay function as (Kirk, 1994; Simonot & Treut, 1986)

$$T_{VSR} = e^{-K_{VSR}(z) \times z}. \tag{2}$$

Here z (m) is the water depth from surface and K_{VSR} (m^{-1}) is the attenuation coefficient of VSR. K_{VSR} is determined by the absorption and scattering properties of constituents in water, which include water molecules, phytoplankton, and colored dissolved organic matters (Kirk, 1994; Lee, Du, Arnone, Liew, et al., 2005). To characterize the spatial and temporal variations of K_{VSR}, its measurements in the oceans can be dated back to ~90 years ago (Poole & Atkins, 1929), where a rich publication can be found to describe the relationship between K_{VSR} and water's constituents in the literature (Gallegos & Neale, 2002; Xing et al., 2012; Zaneveld et al., 1993). In addition, there have been remote sensing algorithms developed to estimate K_{VSR} from the measurement of water (ocean) color (Morel, 2009; Smith et al., 1989; Wei & Lee, 2013).

However, before the widely available K_{VSR} data of the oceans from sophisticated optical-electronic instruments or ocean color remote sensing, the transmittance of solar radiation in water was generally determined based on water types (Jerlov, 1976), where an e folding depth (ξ; m) is assigned for a given water type (Paulson & Simpson, 1977). For instance, in the widely used ROMS, the transmittance of solar radiation in the 400–1000 nm is modeled as (Paulson & Simpson, 1977)

$$T^{PS77}(400-1,000) = R\,e^{-z/\xi_1} + (1-R)\,e^{-z/\xi_2}, \tag{3}$$

where R is a model constant and is approximated as ~0.62 (Paulson & Simpson, 1977). With values for ξ_1 and ξ_2 known for a given water type, the vertical distribution of solar radiation in the 400–1,000 nm is obtained. This system has been applied in dynamic ocean models, such as ROMS, for more than three decades (Oberhuber, 1992; Simonot et al., 1988).

However, water type is a vague and qualitative term for the status of a water body, and the limited 14 types (Jerlov, 1976) cannot cover the fine variations of the various oceanic environments. As a result, the assigned ξ_1 and ξ_2 values may not well represent the attenuation of solar radiation for a water body under study. Secchi disk depth (Z_{SD}; m), on the other hand, is a measure of water's transparency (Lee, Shang, et al., 2015). As indicated in Paulson and Simpson (1977) and Simonot and Treut (1986), use of Z_{SD} can be a practical alternative to get quantitative determination of T_{VSR}, especially for the days before modern ocean optics where the only available measurements of ocean's optical properties was Z_{SD}. Further, the global Z_{SD} (Arnone et al., 1984; Boyce et al., 2012; Frederick, 1970) collected in the past ~150 years show much more detailed spatial variations of the ocean's transparency. However, there have been no studies to estimate T_{VSR} using Z_{SD} as the input based on radiative transfer. Decades ago Simonot and Treut (1986) used a simple empirical relationship to convert Z_{SD} to K_{VSR}, and they treated K_{VSR} as a constant vertically that is not supported by radiative transfer. Here based on a sound theory regarding Secchi disk observation (Lee, Shang, et al., 2015) and the robust relationship between Z_{SD} and the diffuse attenuation coefficient (Lee et al., 2018; Lee, Shang, et al., 2015), as well as a model for the vertical variation of K_{VSR} based on radiative transfer (Lee, Du, Arnone, Liew, et al., 2005), a scheme is developed to use Z_{SD} as the input to model T_{VSR}. The

resulted transmittance values are further evaluated using both simulated data and in situ measurements. This model then opens the door to accurately estimate T_{VSR} of the oceans in the past 100+ years for use in ocean circulation models.

2. Models of K_{VSR} and Z_{SD}

Historically, the attenuation coefficient K_{VSR} has been considered as a constant vertically (Kirk, 1994; Simonot & Treut, 1986; Smith & Baker, 1978). Due to the spectrally selective absorption and scattering coefficients, K_{VSR} also changes with depth (Lee, Du, Arnone, Liew, et al., 2005; Morel, 1988). Various approaches have been considered to take into account this vertical feature, which include multiple exponential terms (Morel & Antoine, 1994; Ohlmann & Siegel, 2000) and a single exponential term but explicitly modeling K_{VSR} as a function of z (Lee, Du, Arnone, Liew, et al., 2005). A recent study (Zoffoli et al., 2017) shows that the model of K_{VSR} as a function of the inherent optical properties (IOPs) and z worked best for both oceanic and coastal waters. We thus here use this K_{VSR} model as the base for the incorporation of Z_{SD}.

Based on Hydrolight simulations of radiative transfer, it is found that K_{VSR} can be well described as (Lee, Du, Arnone, Liew, et al., 2005)

$$K_{\text{VSR}} = K_1 + \frac{K_2}{(1+z)^{0.5}}, \tag{4}$$

where K_1 and K_2 are functions of water's IOPs and Sun angle. Basically K_1 represents the attenuation coefficient of VSR in deeper waters where K_{VSR} depends less on depth, while K_2 represents the attenuation coefficient of VSR in surface layer where K_{VSR} varies significantly. This dependence of K_{VSR} on depth, as detailed in Lee, Du, Arnone, Liew, et al. (2005), is because that highly attenuating photons of VSR (such as those in the red and near-infrared bands) quickly lost in the surface, and only the lest attenuating photons can penetrate to deeper depths. Both K_1 and K_2 still vary with water constituents. In Lee, Du, Arnone, Liew, et al. (2005), K_1 and K_2 were modeled as functions of absorption (a; m^{-1}) and backscattering (b_b; m^{-1}) coefficients at 490 nm, respectively,

$$K_1(\text{IOP}) = \chi_0 + \chi_1 (a(490))^{0.5} + \chi_2 b_b(490), \tag{5a}$$

$$K_2(\text{IOP}) = \varsigma_0 + \varsigma_1 a(490) + \varsigma_2 b_b(490). \tag{5b}$$

The values of $\chi_{0,1,2}$ and $\varsigma_{0,1,2}$ are independent of both depth and water properties, although they may still vary with solar zenith angle (Lee, Du, Arnone, Liew, et al., 2005).

Recently, through thorough analysis and derivations from radiative transfer, it is found, and validated, that Z_{SD} can be robustly modeled as (Lee et al., 2018; Lee, Shang, et al., 2015)

$$Z_{\text{SD}} \approx \frac{0.96}{K_d^{tr}}, \tag{6}$$

where K_d^{tr} is the water's attenuation coefficient at the transparent window (Lee, Shang, et al., 2015). Because K_d is a function of a and b_b (Gordon, 1989; Lee, Du, & Arnone, 2005), we thus see that Z_{SD} is also a function of a and b_b. Therefore, in principle, K_1 and K_2 can be functions of Z_{SD}, and one of the goals of this effort is to parameterize these functions.

3. Data

3.1. Simulated Data

The widely used numerical model Hydrolight (Albert & Mobley, 2003; McKee et al., 2007; Mobley & Sundman, 2013; Stramska & Stramski, 2005) was used to simulate hyperspectral (350–800 nm, 5-nm step) light field in the upper water column for a wide range of IOPs. Details of the setups for these Hydrolight simulations can be found in Lee et al. (2018). Briefly, to simulate subsurface light field with Hydrolight, it is required to provide absorption and scattering coefficients, in addition to boundary conditions such as wind speed, Sun position, and sky conditions. For these simulations, without loss of generality, wind speed was set as 5 m/s, Sun angle was 30° from zenith, and the sky was clear of clouds with a visibility at 30 km.
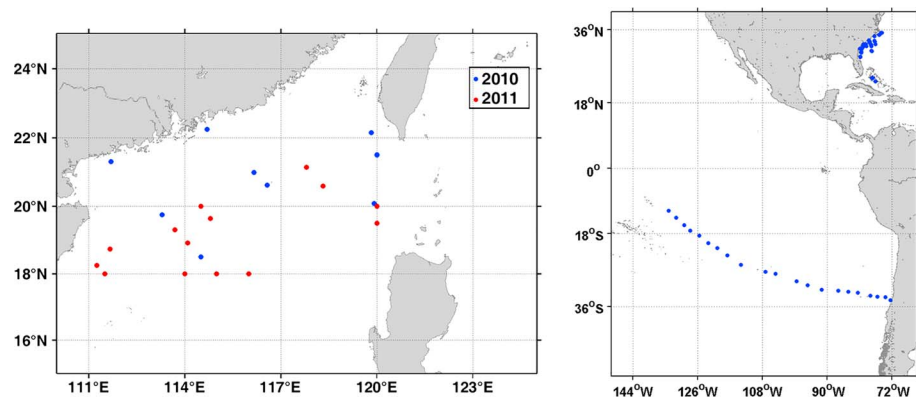
Figure 1. Locations of in situ data used to evaluate models of T_{VSR}.

The absorption coefficient is a sum of the contributions of pure seawater (a_w), phytoplankton (a_{ph}), detritus sediment (a_{dm}), and gelbstoff (a_g; IOCCG, 2000; Mobley, 1994). Values of a_w were taken from the combinations of Sogandares and Fry (1997), Lee, Wei, et al. (2015), and Pope and Fry (1997). To cover waters from oceanic blue to coastal brown waters, a total of 720 a_{ph} spectra were selected from ~4,000 measurements submitted to SeaBASS (the SeaWiFS Bio-optical Archive and Storage System), with the resulted a_{ph}(440) in a range of ~0.0014–39.0 m^{-1}. Further, constrained random spectra of a_{dm} and a_g were modeled based on values of a_{ph}(440) (IOCCG-OCAG, 2003).

The (back)scattering coefficient is a sum of the contributions of pure seawater (b_w), phytoplankton (b_{ph}), and suspended sediments (b_m). Values of b_w were from Zhang et al. (2009), while spectra of b_{ph} and b_m were modeled, random but constrained within ranges from field observations, based on values of a_{ph}(440) (IOCCG-OCAG, 2003). The phase function for detritus/sediment scattering was the averaged Petzold phase function (Mobley, 1994; Petzold, 1972) with a backscattering ratio of 1.83%; the phase function for phytoplankton scattering was a Fournier and Forand function (Fournier & Forand, 1994) with a backscattering ratio of 1%.

With the above setup, 720 sets of IOP spectra were synthesized, where the values of a(490) and b_b(490) varied in a range of ~0.015–50.0 and ~0.002–3.0 m^{-1}, respectively. The component absorption and backscattering coefficients (e.g., a_{dm}, a_g) were not determined by concentration of chlorophyll, so the data set is not "Case-1" in nature. As a result, there is wide range of b_b/a ratio. Such a setup of the input IOPs ensures a broad representation of natural variations. From the simulated light field, the spectrum of the diffuse attenuation coefficients of downwelling irradiance (K_d; m^{-1}) for each set of IOPs was calculated from the simulated irradiance profiles ($E_d(z)$). Further K_d^{tr} of this set of IOPs was determined as the minimum of K_d in the 400–700-nm range; Z_{SD} was subsequently calculated from K_d^{tr} following equation (6).

From these simulations, $T_{VSR}(z)$ was also calculated from the simulated VSR based on equation (1), which is defined as the spectrally integrated E_d in the 400–700-nm range.

3.2. In Situ Measurements

Two sets of in situ measurements were used to evaluate the Z_{SD} scheme for T_{VSR}, with Figure 1 showing the locations of these measurements. One set comprises of measurements made in the South China Sea in 2010 and 2011 (termed SCS data in the following), while the other for data presented in Zoffoli et al. (2017) covering measurements made in the Atlantic and Pacific Oceans (termed APO data in the following).

A total of 23 stations were compiled to have concurrent measurements of Z_{SD} and vertical profiles of solar radiation in the South China Sea, which spans a Z_{SD} range of ~5–25 m (Chl in a range of ~0.5–15 mg/m^3). Z_{SD} followed the conventional approach that used a white disk (30 cm in diameter) tied to a rope and weight. Hyperspectral $E_d(\lambda)$ and upwelling radiance ($L_u(\lambda)$) in the 350–800-nm range were measured with the free-falling HyperPro II Profiler (Satlantic, Inc.), where the entire system was 30–50 m away from the operating boat; thus, the impact of operating boat to the measured vertical profiles of solar radiation is negligible. Quality control of the measured vertical profiles was carried out following the commonly adopted protocol and the data processing software (Prosoft, Satlantic, Inc.) provided by the company. $E_d(z,\lambda)$ profiles were
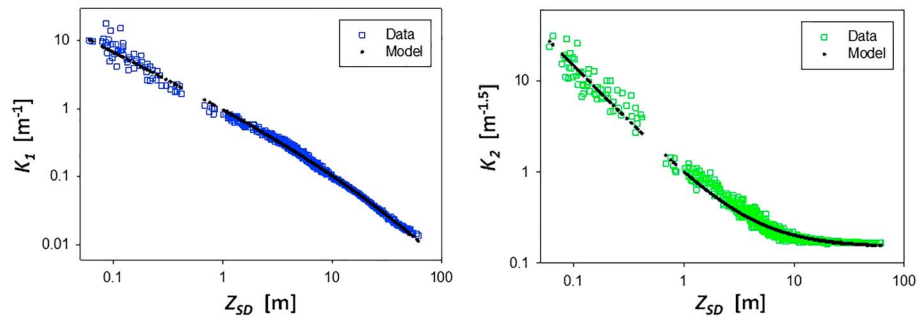
Figure 2. Relationships between Z_{SD} and model parameters K_1 and K_2 for K_{VSR}.

normalized by downwelling irradiance measured above the surface $E_s(0^+,\lambda)$ to correct for any impact from sky light variations, and $\ln(E_d(0,\lambda))$ was estimated as the intercept between $\ln(E_d(z,\lambda))$ and z in a linear regression. Subsequently, $E_{VSR}(z)$ and $E_{VSR}(0)$ were calculated as a spectral integration of $E_d(z,\lambda)$ and $E_d(0,\lambda)$, respectively, for wavelengths of 400–700 nm, and T_{VSR} was then calculated as the ratio of $E_{VSR}(z)/E_{VSR}(0)$. Remote sensing reflectance (R_{rs}; sr^{-1}) of this data set was determined from the above-water approach (Mueller et al., 2003) with a GER-1500 spectral radiometer, where the spectral range is ~350–1,100 nm, with a spectral resolution ~3 nm.

The APO data comprise of 57 stations having hyperspectral E_d profiles (350–800 nm) and R_{rs} collected in the Subtropical Gyre of South Pacific (Z_{SD} is ~75 m) and coastal waters along the Pacific Ocean, North Atlantic Ocean, and Bahamas, encompassing waters in a wide range of transparency (more detailed description can be found in Zoffoli et al. (2017)). Similar to the SCS data set, $E_{VIS}(z)$ and $E_{VIS}(0)$ were obtained as the spectral integral of $E_d(z,\lambda)$ and $E_d(0,\lambda)$, respectively, over the 400–700-nm range after quality control of the measurements (Zoffoli et al., 2017), and $T_{VSR}(z)$ was calculated as $E_{VSR}(z)/E_{VSR}(0)$. There are limited stations of the APO data having concurrent Z_{SD} measurements; therefore, Z_{SD} for each $T_{VSR}(z)$ for this data set was derived from the concurrent R_{rs} spectrum following the scheme described in Lee, Shang, et al. (2015). For these stations, R_{rs} spectra were derived from the HyperPro measurements using the ProSoft software. This is a result of the vertical profiles of upwelling radiance and downwelling irradiance obtained by the HyperPro free-falling optical profiler, and ProSoft derives water-leaving radiance (L_w) and downwelling irradiance just above the surface ($E_d(0+)$) from such profiling measurements, and R_{rs} is the ratio of L_w to $E_d(0+)$. Further, absorption and backscattering coefficients were derived from these R_{rs} following QAA (Lee et al., 2002), and values of Z_{SD} were then calculated following equation (6).

4. Results

4.1. Model Coefficients of T_{VSR} Based on Z_{SD}

For each set of Hydrolight simulations, K_1 and K_2 of equations (5a) and (5b) were calculated from the known $a(490)$ and $b_b(490)$ values. These K_1 and K_2 were further compared with the calculated Z_{SD} following equation (6)). Figure 2 shows K_1 versus Z_{SD} and K_2 versus Z_{SD}, respectively, where K_1 and K_2 appear decreasing with the increase of Z_{SD}, but K_2 approaching a constant for Z_{SD} deeper than ~10 m. K_1 represents mainly K_{VSR} in the deeper depths, so, inversely related to Z_{SD}. K_2, however, represents K_{VSR} in the surface layer where the contribution of pure seawater can be significant. Therefore, for more clear waters (greater Z_{SD} values), K_2 will be mainly from the absorption of pure seawater, and thus approaches a constant.

It is found that there are strong ($R^2 > 0.90$) relationships between the parameters of each pair. Through least squares fitting, both K_1 and K_2 were modeled as a function of Z_{SD}:

$$K_1 = 10^{\alpha_0+\alpha_1 X+\alpha_2 X^2+\alpha_3 X^3}, \tag{7a}$$

$$K_2 = \beta_0 + \beta_1(Z_{SD})^{\beta_2}, \tag{7b}$$

with $X = \ln(Z_{SD})$. Table 1 lists the values for coefficients $\alpha_{0,1,2,3}$ and $\beta_{0,1,2}$. On average, the relative difference between IOPs calculated K_1 and Z_{SD} modeled K_1 is 5.8%, while the relative difference for K_2 is 9.1%.

Table 1
Model Coefficients for K_1 and K_2 Using Z_{SD} Derived From Hydrolight Simulations

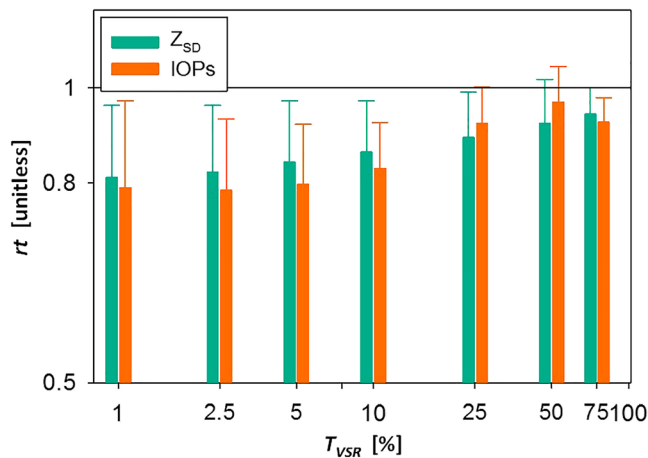|	K_1		K_2
α_0	−0.0136	β_0	0.1511
α_1	−0.8837	β_1	0.8596
α_2	−0.0644	β_2	−1.2295
α_3	−0.0251		

4.2. Evaluation of T_{VSR} Using Simulated Data

Further, to characterize the performance of modeling T_{VSR}, modeled T_{VSR} with the combination of equations (2) and (5a) and (5b) and equations (2), (4), and (7a) and (7b), respectively, were compared with known T_{VSR} obtained from Hydrolight simulations. This comparison is limited to a range of $T_{VSR} \geq 1\%$ though, as the contribution of solar radiation lower than 1% surface VSR has limited impact on heating and photosynthesis (Sathyendranath & Platt, 1989, 1995); also, it is difficult to obtain accurate T_{VSR} in the field for $T_{VSR} < 1\%$ (Zoffoli et al., 2017). As values of T_{VSR} span 2 orders of magnitude, a metrics to quantify the agreement between known and modeled T_{VSR} is calculated as

$$rt = \frac{T_{VSR}^{mod}}{T_{VSR}^{known}}. \tag{8}$$

Median and standard deviation of rt are calculated for interested data pool. This rt value thus indicates how far the modeled T_{VSR} is away from known (or measured) T_{VSR} and also provides an indication if the modeled T_{VSR} is systematically overestimated or underestimated. Using median value, rather than mean, avoids the distortion by a few extreme values (extremely high or low ratios due to measurement errors or uncertainties) that can happen in field measured data.

Overall, it is found that for $T_{VSR} > 1\%$, the median rt value for T_{VSR} modeled by either IOPs ($a(490)$ and $b_b(490)$) or Z_{SD} is ~0.84 (±0.13) and 0.87 (±0.13), respectively ($rt = 1.0$ for perfect agreement) indicates nearly the same performance of using these two schemes to get T_{VSR}. Realizing that this median rt value just represents an overall performance for T_{VSR} in a wide range, but different T_{VSR} values have different impacts on heating and photosynthesis, median rt values (and standard deviation) for T_{VSR} as 1% (0.9–1.1%), 2.5% (2.2–2.8%), 5% (4.5–5.5%), 10% (9–11%), 25% (22–28%), 50% (45–55%), and 75% (70–80%), respectively, were also evaluated (see Table 2). The use of a narrow range of rt is to ensure the collection of more data points, as it may not have measurements fall on exactly, for example, 5%. Figure 3 shows the resulting median rt values for each T_{VSR} range and for models using IOPs and Z_{SD}, respectively. For these seven scales of T_{VSR}, it is found that the median rt values are in a range of ~0.8–1.0, with nearly identical median rt at each scale for both Z_{SD} and IOP approaches (see Figure 3). These results further demonstrate that the outcomes of T_{VSR} modeled using Z_{SD} (equations (7a) and (7b)) is equivalent to that modeled using IOPs (equations (5a) and (5b)), thus supporting the application of Z_{SD} to model T_{VSR}. Also, the similar performance between using Z_{SD} and IOP approaches highlights the nature that both Z_{SD} and the IOPs provide a measure of the diffuse attenuation coefficient of VSR. On the other hand, the less than 1.0 median rt (~0.8–0.9) for $T_{VSR} \leq 10\%$ suggests a slight data dependency of the Lee, Du, Arnone, Liew, et al. (2005) model, which could be further refined after a development of more inclusive data sets, which is out the scope of this study though.

4.3. Evaluation of T_{VSR} Using In Situ Data

As for any model, it is important to evaluate the performance of T_{VSR} using Z_{SD} as the input in the real environment. We applied this scheme to the T_{VSR} measurements of both SCS and APO data sets, with Figure 4 (green bars) showing the resulting median rt values and standard deviation for T_{VSR} in the seven scales as mentioned above. It is found that the median rt values for these data sets are in a range of ~1.5 ± 0.5–1.0 ± 0.1 (SCS) and 3.2 ± 0.7–1.02 ± 0.04 (APO) for the seven scales of T_{VSR} (see Table 3). Not surprisingly, the discrepancies are larger than that of the simulated data, which is mainly due to errors or uncertainties in the measured T_{VSR}, where impacts from clouds cannot be completely removed. In particular, wave focusing or defocusing can cause large uncertainties in $E_d(z)$ (Stramski & Legendre, 1992; Wei et al., 2014), which will then impact the calculated T_{VSR} from in situ

Table 2
Median (Standard Deviation) of rt Corresponding to T_{VSR} Values by Different T_{VSR} Models

T_{VSR} (%)	By Z_{SD}	By IOPs
75	0.94 (0.06)	0.92 (0.05)
50	0.92 (0.10)	0.97 (0.08)
25	0.89 (0.10)	0.92 (0.08)
10	0.86 (0.11)	0.83 (0.09)
5	0.84 (0.13)	0.80 (0.12)
2.5	0.82 (0.14)	0.79 (0.14)
1	0.81 (0.18)	0.79 (0.18)

Note. Hydrolight simulated data.

Figure 3. Median and standard deviation of *rt* values for the seven scales of T_{VSR}, for data from Hydrolight simulations.

measurements. Note that these median *rt* values also include impacts resulting from uncertainties or errors in the measured or R_{rs}-derived Z_{SD} (for the APO data set) where a 15% deeper Z_{SD} can result in ~30% increase in *rt* for T_{VSR} at 10%. The close to 1.0 median *rt* values for these waters for T_{VSR} in a range of 10–75%, however, suggest no systematic errors in the Z_{SD} values used.

Overall, these *rt* values (at least for T_{VSR} greater than 5%) indicate very good agreement between measured and modeled T_{VSR} with Z_{SD} as the sole input. In particular, it covers Z_{SD} from coastal turbid waters to the "clearest" natural waters of the South Pacific Gyre (Morel et al., 2007). Even for an *rt* value of 1.5 at T_{VSR} of 1%, the "true" T_{VSR} is just ~1.5 times lower of the modeled T_{VSR}, suggesting a reasonable estimation for use with dynamic ocean circulation models. This large discrepancy happens at the bottom of the euphotic zone defined by solar radiation. Thus, its impact to the estimation of photosynthesis and heating of the upper water column is limited (Lee et al., 1996; Sathyendranath & Platt, 1995).

Further, we also evaluated, and compared, the performance of T_{VSR} modeled based on the traditional Jerlov water types for these data sets from field measurements, where T_{VSR} is converted from T^{PS77} following

$$T_{VSR}^{PS77} = T^{PS77}(400-1,000)/0.65, \qquad (9)$$

where 0.65 is a constant to account for that surface solar radiation in the 400–700 nm is ~65% of that in the range of 400–1,000 nm, and further that solar radiation in the 700–1,000-nm range has a very shallow (< ~1 m) penetration depth (Morel & Antoine, 1994). The ξ_1 and ξ_2 values required in equation (3) were derived following the approach of Morel (1988) from the measured R_{rs}, where values of Chl were first estimated, and water types were then assigned based on the estimated Chl value.

The orange bars in Figure 4 show the median and standard deviation of *rt* when T_{VSR} is modeled based on the scheme proposed in Paulson and Simpson (1977) (equations (3) and (9)), and termed as PS77 in the following. For the SCS data set, the median *rt* values are ~0.7 ± 0.1–0.9 ± 0.1 by the PS77 model for the seven scales of T_{VSR}, while they are ~0.04 ± 1.8–0.8 ± 0.2 for the APO data set (also see Table 3). Clearly, the comparisons show that T_{VSR} via Z_{SD} is much more consistent with the measured T_{VSR} profiles than that modeled using water type information. The less than 0.1 median *rt* value suggests that T_{VSR} is significantly (10 times or more) underestimated. In addition to the simplicity nature of the PS77 scheme, the significantly lower median *rt* values for T_{VSR} by the PS77 model are likely because the data used to develop PS77 were from a small area that did not cover waters with wide range of transparency. The deepest Z_{SD} presented in PS77 is about 25 m (in a range similar to that of the SCS data set), but ocean waters can have Z_{SD} as deep as ~75 m
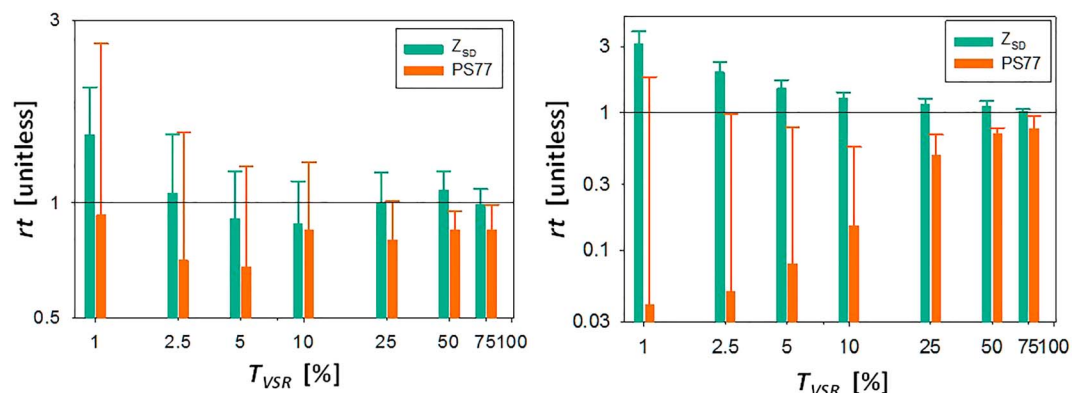
Figure 4. Same as in Figure 3 but for data from field measurements.

Table 3
Median (Standard Deviation) of rt Corresponding to T_{VSR} Values by Different T_{VSR} Models

T_{VSR} (%)	SCS		APO	
	By Z_{SD}	By PS77	By Z_{SD}	By PS77
75	0.99 (0.10)	0.85 (0.14)	1.02 (0.04)	0.76 (0.18)
50	1.08 (0.13)	0.85 (0.10)	1.12 (0.09)	0.7 (0.07)
25	1.0 (0.2)	0.8 (0.21)	1.14 (0.13)	0.49 (0.20)
10	0.88 (0.26)	0.85 (0.43)	1.28 (0.13)	0.15 (0.41)
5	0.91 (0.30)	0.68 (0.57)	1.5 (0.23)	0.08 (0.70)
2.5	1.06 (0.45)	0.71 (0.82)	1.98 (0.37)	0.05 (0.92)
1	1.51 (0.5)	0.93 (1.68)	3.16 (0.74)	0.04 (1.78)

Note. Measured data.

(e.g., in the South Pacific Gyre; Boyce et al., 2012; Lee et al., 2018) where a larger ξ_2 value is required for the PS77 model for such blue waters. With the current ξ_2 value (~20 m) designed for open ocean (Jerlov water type I; Paulson & Simpson, 1977), T_{VSR} is thus significantly (~2–30 times) underestimated for $T_{VSR} < $ ~25%. In dynamic ocean circulation models, this underestimate of T_{VSR} would lead to shallower penetrating depth; thus, the energy of solar radiance would be absorbed in upper layer, resulting in higher (up to ~2 °C) sea surface temperature and shallower (up to ~20 m) mixed layer depth (Murtugudde et al., 2002).

5. Discussion

It has been realized for decades (Lewis et al., 1990; Sathyendranath et al., 1991; Zaneveld et al., 1981) that the penetration of visible solar radiation in the upper water column can affect the upper layer dynamics of the oceans and the ocean–atmosphere system (Gnanadesikan & Anderson, 2009), and this process depends on both surface solar radiation (Shulman et al., 2017) as well as the propagation of solar light through the upper water column (Ohlmann, 2003; Siegel et al., 1995). Surface solar radiation depends on the Sun-Earth orbit, atmospheric properties, and information on cloud; propagation through water column, on the other hand, is governed by water properties (Gordon, 1989; Sathyendranath & Platt, 1988). To accommodate large-scale modeling of this effect, especially to balance the accuracy and computation cost, a wide range of models have been developed in the past decades to estimate the vertical profiles of VSR in the upper water column (Kara et al., 2005; Lee, Du, Arnone, Liew, et al., 2005; Morel & Antoine, 1994; Ohlmann & Siegel, 2000; Ohlmann et al., 2000). Due to its simplicity and the availability of Jerlov water types of the global oceans decades ago (Simonot & Treut, 1986), the PS77 model has been incorporated in the widely used ROMS and HYCOM to account for the contribution and impact of visible solar light. However, because the determination of water type is quite arbitrary and the subtle changes of water's optical properties within a water type is ignored, various studies have shown that the PS77 model for T_{VSR} is obsolete (Murtugudde et al., 2002; Ohlmann, 2003), and more accurate models (Lee, Du, Arnone, Liew, et al., 2005; Morel & Antoine, 1994) have been developed to propagate VSR in the upper water column, especially to incorporate the products of global oceans generated from ocean color satellites.

On the other hand, to get a more reliable characterization and understanding of the changes of the ocean(−atmosphere) systems under a changing climate, it is required to have observations, and evaluations, in multidecadal scales (Boyce et al., 2010; Deser & Blackmon, 1993; Henson et al., 2009). While we are having more and more data from multiple observation systems and advanced satellites that would be critical to study the changes of the coming decades, characterizing and understanding what happened to the ocean–atmosphere systems so far would provide us the needed information/knowledge for present-day policies. For this, there is actually a data pool of the ocean's transparency that can be dated back ~150 years, which could help us to evaluate the impact of solar penetration in the past decades to centuries if such data can be adequately incorporated into dynamic circulation models. To enable this opportunity, here, a model to estimate T_{VSR} based on Z_{SD} is developed. As presented, the estimated T_{VSR} is found matching the measured T_{VSR} very well for waters from the coast waters to the super clear South Pacific Gyre, and the mathematical form makes the computation cost the same as that of the PS77 model. It is also required to know solar radiation at sea surface to run dynamic ocean circulation models, however. The results of Z_{SD}-based T_{VSR} call for the development of accurate solar radiation at sea surface in the past decades to a century. It is envisioned that we may greatly expand our knowledge and understanding of the impact of visible solar radiation to the ocean and atmosphere systems in the past century when a database of global Z_{SD} and surface solar radiation is available.

6. Conclusions

Based on the nature that Secchi disk depth is governed by the attenuation coefficient at the transparent window (Lee, Shang, et al., 2015), and that this attenuation is related to the attenuation in the broad visible band (Lee et al., 2018), a model to estimate T_{VSR} in the upper water column (down to $T_{VSR} = 1$%) based on

radiative transfer and Z_{SD} is developed. Application of this model to estimate T_{VSR} of coastal and oceanic waters show very good agreement with measured T_{VSR}, and this agreement is significantly better than that of the widely used water-type-based model in the past decades, where the latter is implemented in ocean general circulation models. The results here show the tremendous value of the ~150 years of global Z_{SD} data that were the only available optical measurements of the oceans decades to hundred years ago, and evaluation of the oceans through incorporating such data is expected to reveal new features of the oceans in a time scale much longer than that with data from the modern instrumentations.

References

Albert, A., & Mobley, C. D. (2003). An analytical model for subsurface irradiance and remote sensing reflectance in deep and shallow case-2 waters. *Optics Express*, *11*(22), 2873–2890. https://doi.org/10.1364/OE.11.002873

Arnone, R. A., Tucker, S. P., & Hilder, F. A. (1984). Secchi depth atlas of the world coastlines, paper presented at Ocean Optics VII, Proc. SPIE 0489, Monterey, CA, September 27.

Boyce, D. G., Lewis, M., & Worm, B. (2012). Integrating global chlorophyll data from 1890 to 2010. *Limnology and Oceanography: Methods*, *10*(11), 840–852. https://doi.org/10.4319/lom.2012.10.840

Boyce, D. G., Lewis, M. R., & Worm, B. (2010). Global phytoplankton decline over the past century. *Nature*, *466*(7306), 591–596. https://doi.org/10.1038/nature09268

Deser, C., & Blackmon, M. L. (1993). Surface climate variations over the North Atlantic Ocean during winter: 1900–1989. *Journal of Climate*, *6*(9), 1743–1753. https://doi.org/10.1175/1520-0442(1993)006<1743:SCVOTN>2.0.CO;2

Falkowski, P. G., & Wilson, C. (1992). Phytoplankton productivity in the North Pacific Ocean since 1900 and implications for absorption of anthropogenic CO_2. *Nature*, *358*(6389), 741–743. https://doi.org/10.1038/358741a0

Fournier, G. R., & Forand, J. L. (1994). *Analytic phase function for ocean water*. Paper presented at Ocean Optics XII, SPIE, Bergen, Norway, June 13.

Frederick, M. A. (1970). An atlas of Secchi disc transparency and Forel-Ule color codes for the oceans of the world (Rep., 177 pp.). Naval Postgraduate School, Monterey, CA.

Frouin, R., Lingner, D. W., Gautier, C., Baker, K. S., & Smith, R. C. (1989). A simple analytical formula to compute clear sky total and photosynthetically available solar irradiance at the ocean surface. *Journal of Geophysical Research*, *94*(C7), 9731–9742. https://doi.org/10.1029/JC094iC07p09731

Gallegos, C. L., & Neale, P. J. (2002). Partitioning spectral absorption in case 2 waters: Discrimination of dissolved and particulate components. *Applied Optics*, *41*(21), 4220–4233. https://doi.org/10.1364/AO.41.004220

Gnanadesikan, A., & Anderson, W. G. (2009). Ocean water clarity and the ocean general circulation in a coupled climate model. *Journal of Physical Oceanography*, *39*(2), 314–332. https://doi.org/10.1175/2008JPO3935.1

Gordon, H. R. (1989). Can the Lambert-Beer law be applied to the diffuse attenuation coefficient of ocean water? *Limnology and Oceanography*, *34*(8), 1389–1409. https://doi.org/10.4319/lo.1989.34.8.1389

Hedström, K. S. (2000). Technical manual for a coupled sea-ice/ocean circulation model (Rep., 110 pp.). Rutgers University.

Henson, S. A., Sarmiento, J. L., Dunne, J. P., Bopp, L., Lima, I., Doney, S. C., et al. (2009). Is global warming already changing ocean productivity? *Biogeosciences Discussions*, *6*(6), 10,311–10,354. https://doi.org/10.5194/bgd-6-10311-2009

IOCCG (2000). Remote sensing of ocean colour in coastal, and other optically-complex, waters. In S. Sathyendranath (Ed.), *Reports of the International Ocean-Colour Coordinating Group, No.3* (126 pp.). Dartmouth, Canada: IOCCG.

IOCCG-OCAG (2003). Model, parameters, and approaches that used to generate wide range of absorption and backscattering spectra*Rep*., International Ocean Colour Coordinating Group. Retrieved from http://www.ioccg.org/groups/OCAG_data.html

Jerlov, N. G. (1976). *Marine Optics*. New York: Elsevier.

Kara, A. B., Wallcraft, A. J., & Hurlburt, H. E. (2005). A new solar radiation penetration scheme for use in ocean mixed layer studies: An application to the Black Sea using a fine resolution HYbrid coordinate ocean model (HYCOM). *Journal of Physical Oceanography*, *35*(1), 13–32. https://doi.org/10.1175/JPO2677.1

Kirk, J. T. O. (1994). *Light & Photosynthesis in Aquatic Ecosystems*. Cambridge: University Press. https://doi.org/10.1017/CBO9780511623370

Lee, Z., Shang, S., Hu, C., Du, K., Weidemann, A., Hou, W., et al. (2015). Secchi disk depth: A new theory and mechanistic model for underwater visibility. *Remote Sensing of Environment*, *169*, 139–149. https://doi.org/10.1016/j.rse.2015.08.002

Lee, Z., Wei, J., Voss, K., Lewis, M., Bricaud, A., & Huot, Y. (2015). Hyperspectral absorption coefficient of "pure" seawater in the range of 350–550 nm inverted from remote sensing reflectance. *Applied Optics*, *54*(3), 546–558. https://doi.org/10.1364/AO.54.000546

Lee, Z. P., Carder, K. L., & Arnone, R. (2002). Deriving inherent optical properties from water color: A multi-band quasi-analytical algorithm for optically deep waters. *Applied Optics*, *41*(27), 5755–5772. https://doi.org/10.1364/AO.41.005755

Lee, Z. P., Carder, K. L., Marra, J., Steward, R. G., & Perry, M. J. (1996). Estimating primary production at depth from remote sensing. *Applied Optics*, *35*(3), 463–474. https://doi.org/10.1364/AO.35.000463

Lee, Z. P., Du, K., Arnone, R., Liew, S. C., & Penta, B. (2005). Penetration of solar radiation in the upper ocean—A numerical model for oceanic and coastal waters. *Journal of Geophysical Research*, *110*, C09019. https://doi.org/10.01029/02004JC002780

Lee, Z. P., Du, K. P., & Arnone, R. (2005). A model for the diffuse attenuation coefficient of downwelling irradiance. *Journal of Geophysical Research*, *110*, C02016. https://doi.org/10.1029/2004JC002275

Lee, Z.-P., Shang, S., Du, K., & Wei, J. (2018). Resolving the long-standing puzzles about the observed Secchi depth relationships. *Limnology and Oceanography*. https://doi.org/10.1002/lno.10940

Lewis, M. R., Carr, M., Feldman, G., Esaias, W., & McClain, C. (1990). Influence of penetrating solar radiation on the heat budget of the equatorial Pacific Ocean. *Nature*, *347*(6293), 543–545. https://doi.org/10.1038/347543a0

McKee, D., Cunningham, A., Wright, D., & Hay, L. (2007). Potential impacts of nonalgal materials on water-leaving Sun induced chlorophyll fluorescence signals in coastal waters. *Applied Optics*, *46*(31), 7720–7729. https://doi.org/10.1364/ao.46.007720

Mellor, G. L. (2002). Users guide for a three-dimensional, primitive equation, numerical ocean model Rep. Princeton University.

Mobley, C. D. (1994). *Light and Water: Radiative Transfer in Natural Waters* (p. 592). New York: Academic Press.

Mobley, C. D., & Boss, E. S. (2012). Improved irradiances for use in ocean heating, primary production, and photo-oxidation calculations. *Applied Optics*, *51*(27), 6549–6560.

Mobley, C. D., Chai, F., Xiu, P., & Sundman, L. K. (2015). Impact of improved light calculations on predicted phytoplankton growth and heating in an idealized upwelling-downwelling channel geometry. *Journal of Geophysical Research: Oceans*, *120*, 875–892. https://doi.org/10.1002/2014JC010588

Mobley, C. D., & Sundman, L. K. (2013). *HydroLight 5.2 User's Guide*. Bellevue, WA: Sequoia Scientific, Inc.

Morel, A. (1988). Optical modeling of the upper ocean in relation to its biogenous matter content (case I waters). *Journal of Geophysical Research*, *93*(C9), 10,749–10,768. https://doi.org/10.1029/JC093iC09p10749

Morel, A. (2009). Are the empirical relationships describing the bio-optical properties of case 1 waters consistent and internally compatible? *Journal of Geophysical Research*, *114*, C01016. https://doi.org/10.1029/2008JC004803

Morel, A., & Antoine, D. (1994). Heating rate within the upper ocean in relation to its bio-optical state. *Journal of Physical Oceanography*, *24*(7), 1652–1665. https://doi.org/10.1175/1520-0485(1994)024<1652:HRWTUO>2.0.CO;2

Morel, A., Gentili, B., Claustre, H., Babin, A., Bricaud, A., Ras, J., & Tieche, F. (2007). Optical properties of the "clearest" natural waters. *Limnology and Oceanography*, *52*(1), 217–229. https://doi.org/10.4319/lo.2007.52.1.0217

Mueller, J. L., Fargion, G. S., & McClain, C. R. (2003). *Ocean Optics Protocols for Satellite Ocean Color Sensor Validation, Revision 4*. Greenbelt, MD: NASA, Goddard Space Flight Center.

Murtugudde, R., Beauchamp, J., McClain, C. R., Lewis, M., & Busalacchi, A. J. (2002). Effects of penetrative radiation on the upper tropical ocean circulation. *Journal of Climate*, *15*(5), 470–486. https://doi.org/10.1175/1520-0442(2002)015<0470:EOPROT>2.0.CO;2

Oberhuber, J. M. (1992). Simulation of the Atlantic circulation with a coupled sea ice-mixed layer-isopycnal general circulation model. Part I: Model description. *Journal of Physical Oceanography*, *23*, 808–829.

Ohlmann, J. C. (2003). Ocean radiant heating in climate models. *Journal of Climate*, *16*(9), 1337–1351. https://doi.org/10.1175/1520-0442-16.9.1337

Ohlmann, J. C., & Siegel, D. (2000). Ocean radiant heating. Part II: Parameterizing solar radiation transmission through the upper ocean. *Journal of Physical Oceanography*, *30*(8), 1849–1865. https://doi.org/10.1175/1520-0485(2000)030<1849:ORHPIP>2.0.CO;2

Ohlmann, J. C., Siegel, D. A., & Mobley, C. D. (2000). Ocean radiant heating. Part I: Optical influences. *Journal of Physical Oceanography*, *30*, 1833–1848.

Paulson, C. A., & Simpson, J. J. (1977). Irradiance measurements in the upper ocean. *Journal of Physical Oceanography*, *7*, 953–956.

Petzold, T. J. (1972). Volume scattering functions for selected natural waters (Rep., pp. 72–78). Scripps Inst. Oceanogr.

Poole, H. H., & Atkins, W. R. G. (1929). Photo-electric measurements of submarine illumination throughout the year. *Journal of the Marine Biological Association of the United Kingdom*, *16*(01), 297–324. https://doi.org/10.1017/S0025315400029829

Pope, R., & Fry, E. (1997). Absorption spectrum (380–700 nm) of pure waters: II. Integrating cavity measurements. *Applied Optics*, *36*(33), 8710–8723.

Sathyendranath, S., Gouveia, A. D., Shetye, S. R., Ravindran, P., & Platt, T. (1991). Biological control of surface temperature in the Arabian Sea. *Nature*, *349*(6304), 54–56. https://doi.org/10.1038/349054a0

Sathyendranath, S., & Platt, T. (1988). The spectral irradiance field at the surface and in the interior of the ocean: A model for applications in oceanography and remote sensing. *Journal of Geophysical Research*, *93*(C8), 9270–9280. https://doi.org/10.1029/JC093iC08p09270

Sathyendranath, S., & Platt, T. (1989). Computation of aquatic primary production: Extended formalism to include effect of angular and spectral distribution of light. *Limnology and Oceanography*, *34*(1), 188–198. https://doi.org/10.4319/lo.1989.34.1.0188

Sathyendranath, S., & Platt, T. (1995). Remote sensing of water-column primary production. In W. K. W. Li & S. Y. Maestrini (Eds.), *Measurement of Primary Production From the Molecular to the Global Scale* (pp. 236–243). Copenhagen: ICES Marine Science Symposia.

Shulman, I., Richard, J., Gould, W., Anderson, S., & Sakalaukus, P. (2017). Impact of errors in short wave radiation and its attenuation on modeled upper ocean heat content. *Journal of Applied Remote Sensing*, *11*(3). https://doi.org/10.1117/1111.JRS.1111.032402

Siegel, D., Ohlmann, J. C., Washburn, L., Bidigare, R. R., Nosse, C. T., Fields, E., & Zhou, Y. (1995). Solar radiation, phytoplankton pigments and radiant heating of the equatorial Pacific warm pool. *Journal of Geophysical Research*, *100*(C3), 4885–4891. https://doi.org/10.1029/94JC03128

Simonot, J.-Y., Dollinger, E., & Treut, H. L. (1988). Thermodynamic-biological-optical coupling in the oceanic mixed layer. *Journal of Geophysical Research*, *93*(C7), 8193–8202. https://doi.org/10.1029/JC093iC07p08193

Simonot, J. Y., & Treut, H. L. (1986). A climatological field of mean optical properties of the world ocean. *Journal of Geophysical Research*, *91*. https://doi.org/10.1029/JC1091iC1005p06642

Smith, R. C., & Baker, K. S. (1978). The bio-optical state of ocean waters and remote sensing. *Limnology and Oceanography*, *23*(2), 247–259. https://doi.org/10.4319/lo.1978.23.2.0247

Smith, R. C., Prezelin, B. B., Bidigare, R. R., & Baker, K. S. (1989). Bio-optical modeling of photosynthetic production in coastal waters. *Limnology and Oceanography*, *34*(8), 1524–1544. https://doi.org/10.4319/lo.1989.34.8.1524

Sogandares, F. M., & Fry, E. S. (1997). Absorption spectrum (340–640 nm) of pure water. I. Photothermal measurements. *Applied Optics*, *36*(33), 8699–8709. https://doi.org/10.1364/AO.36.008699

Stramska, M., & Stramski, D. (2005). Effects of a nonuniform vertical profile of chlorophyll concentration on remote-sensing reflectance of the ocean. *Applied Optics*, *44*(9), 1735–1747. https://doi.org/10.1364/AO.44.001735

Stramski, D., & Legendre, L. (1992). Laboratory simulation of light-focusing by water-surface waves. *Marine Biology*, *114*(2), 341–348. https://doi.org/10.1007/BF00349537

Wei, J., & Lee, Z. P. (2013). Model of the attenuation coefficient of daily photosynthetically available radiation in the upper ocean. *Methods in Oceanography*, *8*, 56–74. https://doi.org/10.1016/j.mio.2013.12.001

Wei, J., Lewis, M. R., Dommelen, R. V., Zappa, C. J., & Twardowski, M. S. (2014). Wave-induced light field fluctuations in measured irradiance depth profiles: A wavelet analysis. *Journal of Geophysical Research: Oceans*, *119*, 1344–1364. https://doi.org/10.1002/2013JC009572

Xing, X., Morel, A., Claustre, H., D'Ortenzio, F., & Poteau, A. (2012). Combined processing and mutual interpretation of radiometry and fluorometry from autonomous profiling Bio-Argo floats: 2. Colored dissolved organic matter absorption retrieval. *Journal of Geophysical Research*, *117*, C04022. https://doi.org/10.1029/2011JC007632

Zaneveld, J. R. V., Kitchen, J. C., & Mueller, J. L. (1993). Vertical structure of productivity and its vertical integration as derived from remotely sensed observations. *Limnology and Oceanography*, *38*(7), 1384–1393. https://doi.org/10.4319/lo.1993.38.7.1384

Zaneveld, J. R. V., Kitchen, J. C., & Pak, H. (1981). The influence of optical water type on the heating rate of a constant depth mixed layer. *Journal of Geophysical Research*, *86*(C7), 6426–6428. https://doi.org/10.1029/JC086iC07p06426

Zhang, X., Hu, L., & He, M.-X. (2009). Scattering by pure seawater: Effect of salinity. *Optics Express*, *17*(7), 5698–5710. https://doi.org/10.1364/OE.17.005698

Zoffoli, M. L., Lee, Z.-P., Ondrusek, M., Lin, J., Kovach, C., Wei, J., & Lewis, M. (2017). Estimation of transmittance of solar radiation in the visible domain based on remote sensing: Evaluation of models using in situ data. *Journal of Geophysical Research: Oceans*, *122*, 9176–9188. https://doi.org/9110.1002/2017JC013209